Nuclear Engineering and Technology 53 (2021) 2788–2802

Contents lists available at ScienceDirect

Nuclear Engineering and Technology

journal homepage: www.elsevier.com/locate/net

Original Article

Use of Monte Carlo code MCS for multigroup cross section generation for fast reactor analysis

Tung Dong Cao Nguyen, Hyunsuk Lee, Deokjung Lee*

Department of Nuclear Engineering Ulsan National Institute of Science and Technology (UNIST), 50 UNIST-gil, Ulsan, 44919, Republic of Korea

ARTICLE INFO

Article history:
Received 29 September 2020
Received in revised form
4 March 2021
Accepted 5 March 2021
Available online 25 March 2021

Keywords:
Monte Carlo
Nodal diffusion
Multigroup
Cross section generation
SFR
MCS

ABSTRACT

Multigroup cross section (MG XS) generation by the UNIST in-house Monte Carlo (MC) code MCS for fast reactor analysis using nodal diffusion codes is reported. The feasibility of the approach is quantified for two sodium fast reactors (SFRs) specified in the OECD/NEA SFR benchmark: a 1000 MW_{th} metal-fueled SFR (MET-1000) and a 3600 MW_{th} oxide-fueled SFR (MOX-3600). The accuracy of a few-group XSs generated by MCS is verified using another MC code, Serpent 2. The neutronic steady-state whole-core problem is analyzed using MCS/RAST-K with a 24-group XS set. Various core parameters of interest (core k_{eff}, power profiles, and reactivity feedback coefficients) are obtained using both MCS/RAST-K and MCS. A code-to-code comparison indicates excellent agreement between the nodal diffusion solution and stochastic solution; the error in the core k_{eff} is less than 110 pcm, the root-mean-square error of the power profiles is within 1.0%, and the error of the reactivity feedback coefficients is within three standard deviations. Furthermore, using the super-homogenization-corrected XSs improves the prediction accuracy of the control rod worth and power profiles with all rods in. Therefore, the results demonstrate that employing the MCS MG XSs for the nodal diffusion code is feasible for high-fidelity analyses of fast reactors.

1. Introduction

Recent expansion in global industry has increased the incentive to design nuclear reactors with enhanced safety features as a sustainable energy source. The sodium fast reactor (SFR) has become one of the most promising reactors to satisfy these criteria, according to the Generation IV International Forum [1]. Owing to the complex behavior of an operating nuclear power reactor, a simulation code system that accurately demonstrates the feasibility of such a reactor is essential. One of the most common approaches is the Monte Carlo (MC) method, which is highly accurate and versatile. However, it requires considerable computational resources and time. A nodal diffusion code, by contrast, can produce a solution more rapidly using fewer computational resources. Theoretically, its results are less accurate than those of MC codes owing to the use of approximations to simplify the model and the strong dependence on the macroscopic cross section (XS). Because it is desirable to develop a sequence that can generate accurate solutions with lower computational and time requirements, the feasibility of coupling the MC and nodal diffusion methods to analyze fast reactors has attracted increasing attention. The fast reactor is selected owing to its longer neutron mean free path compared to thermal reactors, which makes it feasible to use the homogenized XS over a large volume without introducing significant errors. Nikitin et al. [2] recently used the Serpent MC code to prepare homogenized group constants for nodal diffusion analyses using DYN3D and PARCS; the results were verified against the full-core Serpent MC solution. Nikitin and Fridman [3] have conducted extensive research on the use of the Serpent-DYN3D sequence to model the Phenix end-of-life control rod withdrawal tests. Heo et al. [4] performed a similar study using MCNP5 to generate nine-group XS data for the DIF3D code to analyze a 300 MWe SFR transuranic burner core. A general concern with the nodal diffusion method is the unbalanced reaction rate compared to the MC solutions when large local depressions of the flux distribution occur owing to the use of strongly absorbing or toxic materials. Thus, this

* Corresponding author. Department of Nuclear Engineering Ulsan National Institute of Science and Technology, 50 UNIST-gil, Eonyang-eup, Ulju-gun, Ulsan, 44919, Republic of Korea.
E-mail addresses: tungnguyen@unist.ac.kr (T.D.C. Nguyen), hyunsuklee@unist.ac.kr (H. Lee), deokjung@unist.ac.kr (D. Lee).

https://doi.org/10.1016/j.net.2021.03.005

method requires a special technique during generation of the multigroup (MG) XS over a large volume. Nikitin et al. [5] have studied the super homogenization (SPH) method and claimed that it plays an important role in fast reactor analysis of control rod insertion. Sen et al. [6] reported another study on the use of the SPH factor for a hypothetical high-temperature reactor.

Motivated by these studies, Ulsan National Institute of Science and Technology (UNIST) has been developing an MC code, MCS [7–13], that generates MG XSs for the nodal diffusion code RAST-K [14,15] to simulate a liquid-metal-cooled fast reactor. In this work, the few-group macroscopic XSs generated by MCS are first verified against the Serpent 2 [16] solutions. The feasibility of the MCS/RAST-K (MCS/R2) code system is then demonstrated against two typical SFR designs, a modular 1000 MW_{th} metal-fueled SFR (MET-1000) and a large 3600 MW_{th} oxide-fueled SFR (MOX-3600), which are specified in the OECD/NEA SFR benchmark [17]. Several parameters of interest are computed for code-to-code comparison, including the core multiplication factor, power profiles, and reactivity feedback coefficients. Moreover, this work adopts the SPH method to develop a systematic approach to analyzing a fast reactor with all rods in, which is verified for the control rod worth (CRW) against the two benchmark SFR cores.

This paper is organized as follows. In Section 2, the UNIST in-house Monte Carlo code, MCS, and nodal diffusion code, RAST-K, are introduced, and the computer codes used as references are briefly presented. In Section 3, the MET-1000 and MOX-3600 SFR benchmark cores are described. Section 4 briefly introduces the MC method to tally the MG XSs and the verification against Serpent 2. Section 5 presents the approaches to generating the MG XSs for multiplying regions and non-multiplying regions. Then, a code-to-code comparison of the RAST-K results and the whole-core MCS solutions is performed. Finally, the conclusions and future perspectives are discussed in Section 6.

2. Computer codes

Three computers codes are employed: two MC codes, MCS and Serpent 2, and one nodal diffusion code, RAST-K. Serpent 2 is used only to generate homogenized few-group XSs as a reference to verify the MCS solution, which is described in Section 3.

2.1. UNIST Monte Carlo code MCS

MCS is a 3D continuous-energy neutron physics code for particle transport based on the MC method; it has been under development at UNIST since 2013 [7]. MCS can perform criticality runs for reactivity calculations and fixed source runs for shielding problems. MCS was developed from scratch to perform whole-core criticality simulations with pin-wise depletion and thermal/hydraulics (T/H) feedback. The neutron transport capability of MCS has been verified and validated against several benchmark problems, including the BEAVRS benchmark [7], the VERA benchmark [8], ~300 cases from the International Criticality Safety Benchmark Experimental Problem [9], and the OECD/NEA SFR benchmark [10]. MCS is also capable of whole-core simulation with pin-wise depletion and an internal T/H feedback module, and it has been validated against the solutions of BEAVRS [7], VERA [11], OPR-1000 reactors [12], and APR-1400 [13]. XS generation capability was recently added to MCS and is described in this study.

2.2. Monte Carlo code serpent 2

The Serpent code [16] is a continuous-energy MC reactor physics burnup code with recent applications in radiation shielding, multiphysics, and fusion neutronics. It is currently employed for reactor physics applications, including homogenized group constant generation, burnup calculations, the modeling of small research reactor cores, and multiphysics calculations. SERPENT has been under development at the VTT Technical Research Centre of Finland since 2004, and the release of the current development version, Serpent 2, has notably diversified the applications of the code.

2.3. Nodal diffusion code RAST-K

The RAST-K code was developed at UNIST for diffusion core calculations [14]. It adopts the 3D nodal method with the MG coarse mesh finite difference acceleration technique to solve steady-state and transient problems using assembly-level nodes. The triangular polynomial expansion nodal method was recently implemented in RAST-K for fast reactor analysis [15].

3. Benchmark descriptions

To evaluate the accuracy of the XSs generated by MCS, a modular metal-fueled 1000 MW_{th} SFR (MET-1000) and a large mixed-oxide-fueled 3600 MW_{th} SFR (MOX-3600) specified in the OECD/NEA benchmark [17] are selected for analysis.

Figs. 1 and 2 show the radial core layout of the 1000 MW_{th} medium-sized metallic and 3600 MW_{th} large benchmark cores. The MET-1000 core has 180 drivers, 114 radial reflectors, 66 radial shields, and 19 control subassemblies (SAs). It consists of two zones, the inner core zone and outer core zone, which contain 78 and 102 driver assemblies, respectively. Two independent safety-grade reactivity control subsystems are employed. The primary and secondary control systems contain 15 and 4 control SAs, respectively. Each driver SA consists of 271 fuel pins arranged in a triangular pitch array with HT-9 cladding and is enclosed by a hexagonal HT-9 duct. Each fuel rod is divided into four axial zones: the lower reflector, fuel, bond sodium, and gas plenum (Fig. 3a). The radial pattern of the driver assembly is illustrated in Fig. 3b.

The MOX-3600 core is composed of 225 inner and 228 outer MOX fuel SAs depended on the Plutonium content. Each fuel SA contains 271 helium-bonded fuel rods with oxide-dispersion-strengthened steel cladding and is enclosed by a hexagonal EM10 steel duct. The fuel rod is divided into five axial zones: the lower gas plenum, lower reflector, fuel, upper gas plenum, and upper reflector (Fig. 4a). The radial pattern of the fuel SA is illustrated in Fig. 4b. The core is surrounded by 330 radial reflector SAs. The MOX-3000 has two reactivity control systems; the primary control system has 24 control SAs, and the secondary control system has 9 control SAs.

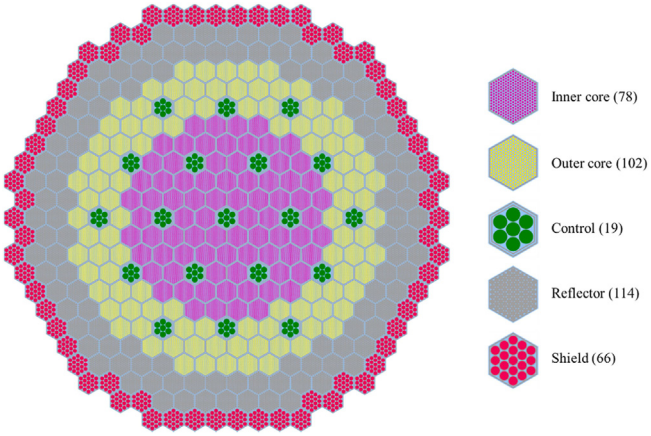

Fig. 1. MET-1000 radial core layout.

Although several materials surround these cores, a vacuum boundary condition is imposed in this study. More detailed descriptions are provided in the OECD/NEA benchmark report [17].

3.1. Monte Carlo methodology for macroscopic cross section generation

The mean neutron flux for a specific geometrical region and for a number of energy ranges (an energy group) is initially calculated by the MC code [18] as a weighting function to tally the targeted XSs:

$$\phi_g = \frac{1}{V}\int_V \mathrm{d}V \int_{E_g}^{E_{g-1}} \mathrm{d}E\phi(r,E) \tag{1}$$

where $\phi(r,E)$ is the space-energy-dependent flux, V is the volume, and g is the group index with upper and lower energy boundaries of E_g and E_{g-1}. Certain reaction rates can be tallied as the product of the estimated flux and the XS of interest, as shown in Eq. (2). The ratio of these two integrals [Eq. (3)] determines the XS for a specific reaction type x and energy group g.

$$R_x = \frac{1}{V}\int_V \mathrm{d}V \int_{E_g}^{E_{g-1}} \mathrm{d}E\Sigma_x(r,E)\phi(r,E) \tag{2}$$

$$\Sigma_{x,g} = \frac{\frac{1}{V}\int_V \mathrm{d}V \int_{E_g}^{E_{g-1}} \mathrm{d}E\Sigma_x(r,E)\phi(r,E)}{\phi_g} \tag{3}$$

where $\Sigma_x(r,E)$ is a space-energy-dependent XS. As discussed, the generated XSs are used in the nodal diffusion code, which obtains a set of XSs, including the total XS, absorption XS, fission XS and fission production, fission spectrum, transport XS, and scattering matrix. Note that, as in the fast reactor simulation, the scalar flux is employed as an approximate weighting function to tally the *Pn* scattering matrix:

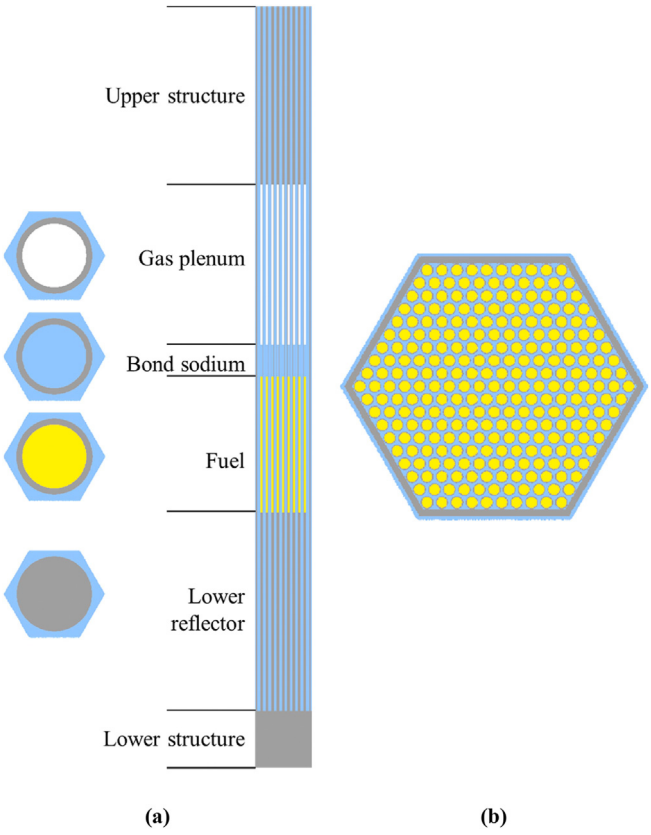

Fig. 3. MET-1000 driver SA: (a) axial layout and (b) radial layout.

$$\Sigma^l_{s,g\to g'} = \frac{\frac{1}{V}\int_V dV \int_{E_g}^{E_{g-1}} dE \int_{E_{g'}}^{E_{g'-1}} dE' \int_{-1}^{1} d\mu\Sigma_s(r,E\to E',\mu)P_l(\mu)\phi(r,E)}{\phi_g} \tag{4}$$

where l is the scattering order, which is also the lth-order Legendre

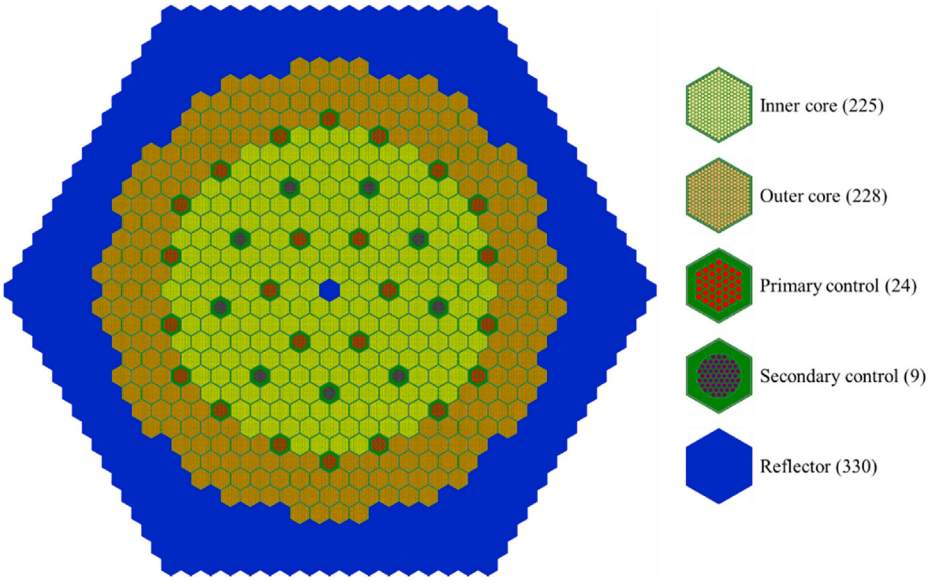

Fig. 2. MOX-3600 radial core layout.

polynomial coefficient, $P_l(\mu)$, and μ is the cosine angle between the incident neutron with energy E and the outgoing neutron with energy E'. The transport XS is then tallied using the outward scattering approximation:

$$\Sigma_{tr,g} = \Sigma_{t,g} - \sum_{g'=1}^{G} \Sigma^1_{s,g\to g'} \tag{5}$$

where G is the total number of groups. The fission spectrum χ_g is defined as the probability distribution over the outgoing fission energy:

$$\chi_g = \frac{\int_{E_g}^{E_{g-1}} dE \int_0^\infty dE' \nu\Sigma_f(r, E'\to E)\phi(r, E')}{\int_0^\infty dE \int_0^\infty dE' \nu\Sigma_f(r, E'\to E)\phi(r, E')} \tag{6}$$

To perform the steady-state simulation, R2 also requires Kappa-fission XS, which is defined as the product of Kappa value (average energy released per fission, $\kappa \approx 200$ MeV/fission) and the fission XS. It is noted that MCS also uses the same κ for all steady-state simulations in this work, resulting in the consistency in MC code MCS and diffusion code R2.

In addition, MCS has an advanced feature, the indices option, that differs from the conventional XS homogenization performed by the MC code Serpent 2. This feature enables MCS to tally the MG XSs for a range of selected cells or meshes separately or simultaneously without repeated calculations or further processing steps. It provides flexible approaches to generating XSs more quickly for multipurpose reactor analysis. While MCS collapses a few-group XSs directly from continuous-energy data, Serpent 2 uses an intermediate MG structure to calculate homogenized few-group constants [16]. However, those intermediate MG XSs are in fact collapsed from the continuous-energy data. Therefore, it might be considered that a roughly consistent approach is used in MCS and Serpent 2. In fact, the same energy structure as 9-group was set for both intermediate fine group and few-group structure in Serpent 2 calculation for better consistency in MCS and Serpent 2.

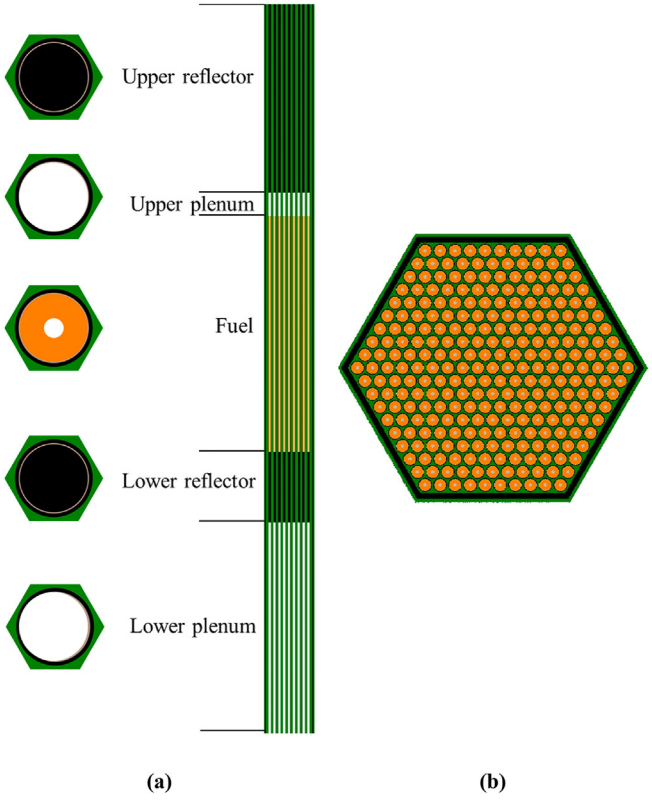

Fig. 4. MOX-3600 driver SA: (a) axial layout and (b) radial layout.

For verification, a nine-group XS set for a 2D assembly problem is generated by MCS and compared to those obtained using Serpent 2. The nine-group energy structure is listed in Table 1. Table 2 summarizes the k_{eff} and the maximum/minimum pin power predicted by MCS and Serpent 2. An excellent agreement is seen with the bias of 2 ± 3 pcm. The additional radial pin-wise power comparison shows the great consistency between two MC codes, with the root mean square (RMS) error is less than 0.03% (as in Fig. 5). Fig. 6 shows the macroscopic nine-group XSs tallied by MCS and their differences from those of Serpent 2. A code-to-code comparison shows excellent agreement between the MCS and Serpent 2 solutions, with all XS errors of less than 0.05%. The groupwise fission spectrum seems to fluctuate compared to the other XSs as the energy group changes from fast to thermal. The reason is an immense probability of fission neutron born in the fast energy range and the rapid growth of the uncertainty of the fission spectrum (it is more than 0.3% for the seventh group and increases to a few percent for the following groups). These fluctuations are, however, still within an acceptable range owing to the extremely small magnitude of the fission spectrum when going to the thermal group in fast reactor analysis.

Figs. 7 and 8 show the P0 and P1 scattering errors, respectively, and their uncertainties (in %) for the MCS and Serpent 2 results. The index in the orange column represents the departure energy group, whereas the green row indicates the arrival energy group. In this investigation, the up-scattering elements and very low-magnitude elements are excluded from the scattering matrices used for comparison owing to their very large uncertainties. Overall, the groupwise scattering XSs given by MCS are quite consistent with those of SERPENT 2, except for the last few groups, which are affected by the lack of neutrons in the thermal energy range. This problem is one of the drawbacks of using an MC technique when too few neutrons are sampled. When the effect of the thermal group XSs on the fast reactor becomes less significant, this defect is negligible. It is also noted that the scattering matrices are highly anisotropic in fast spectrum. When an MC approach is used, it is typically not worth comparing the high-order scattering matrices owing to the very large statistical uncertainties beyond the first order despite being tallied with scalar flux as a weighting function. As an example, the P1 scattering matrix is tallied with respect to the first Legendre polynomial coefficient, $P_1(\mu) = \mu$, where μ is cosine of scattering angle, of which value ranges from −1 to 1. As result, the P1 element is the integration of both positive and negative values, which creates a cancelling effect resulting in the small magnitude

Table 1
Nine-group energy structure.

No.	Upper E (MeV)	Lower E (MeV)
1	1.9640E+01	6.0653E+00
2	6.0653E+00	2.2313E+00
3	2.2313E+00	8.2085E−01
4	8.2085E−01	1.8316E−01
5	1.8316E−01	4.0868E−02
6	4.0868E−02	9.1188E−03
7	9.1188E−03	2.0347E−03
8	2.0347E−03	4.5400E−04
9	4.5400E−04	1.4863E−04

Table 2
Summary of k_{eff} and pin power using MCS and Serpent 2.

Parameter	MCS ($\pm\sigma$)	Serpent ($\pm\sigma$)	Diff. ($\pm\sigma$)
k_{eff}	1.48226 ± 0.00002	1.48228 ± 0.00002	2 ± 3 pcm
Pin power			
– Maximum	1.0028 ± 0.0001	1.0032 ± 0.0002	−0.04 ± 0.03%
– Minimum	0.9966 ± 0.0001	0.9963 ± 0.0002	0.03 ± 0.03%

of many P1 scattering elements. In consequence, the considerable statistical uncertainties are unavoidable.

4. Solutions of the full-core calculations

4.1. Generation of the MG XSs and application of the SPH method

A general approach to tallying the 24-group XSs of each component of the fast reactor is discussed. Table 3 shows the 24-group energy structure. It is noted that a 24-group is a subset of the 33-group structure of the ECCO-33. It is constructed by merging the last 10 thermal energy groups into a single group since MCS calculations give considerable statistical uncertainties in neutron flux for those 10 groups. As mentioned in Section 3, MET-1000 and MOX-3600 have two types of fuel SA: inner and outer. Therefore, the target XSs for each type of fuel SA are obtained using a single 2D model of a fuel SA with reflective boundary conditions. For the non-multiplying regions except radial reflector, all the homogenized XSs are sampled using 2D supercell models, as shown in Fig. 9 [2,3]. To approximate the flux in these regions in the core, they are located at the center of the model and surrounded by the fuel SA. The main purpose of developing this MCS/R2 code sequence is not only for fast reactor benchmarks but also for core design. The 2D model with reflective boundary condition is favorable rather than 3D one owning to the fact that it is independent of the core loading pattern and the total simulation time with 2D models is essentially shorter

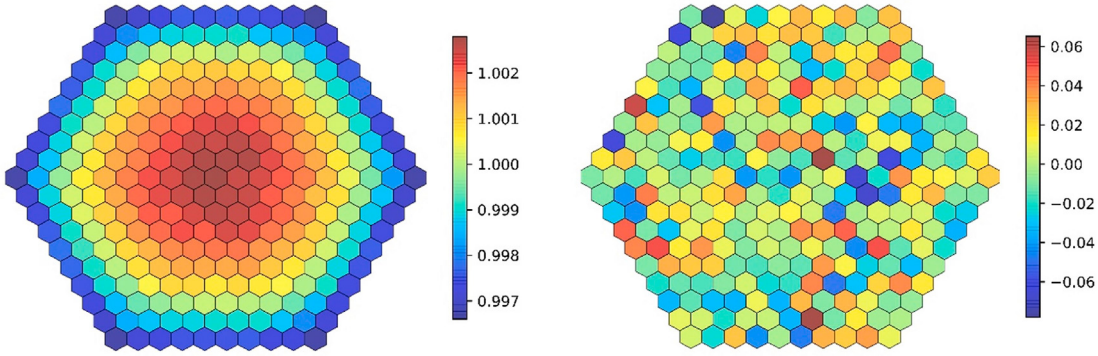

Fig. 5. MCS radial pin-wise power distribution (left) and its error versus Serpent 2 results (right).

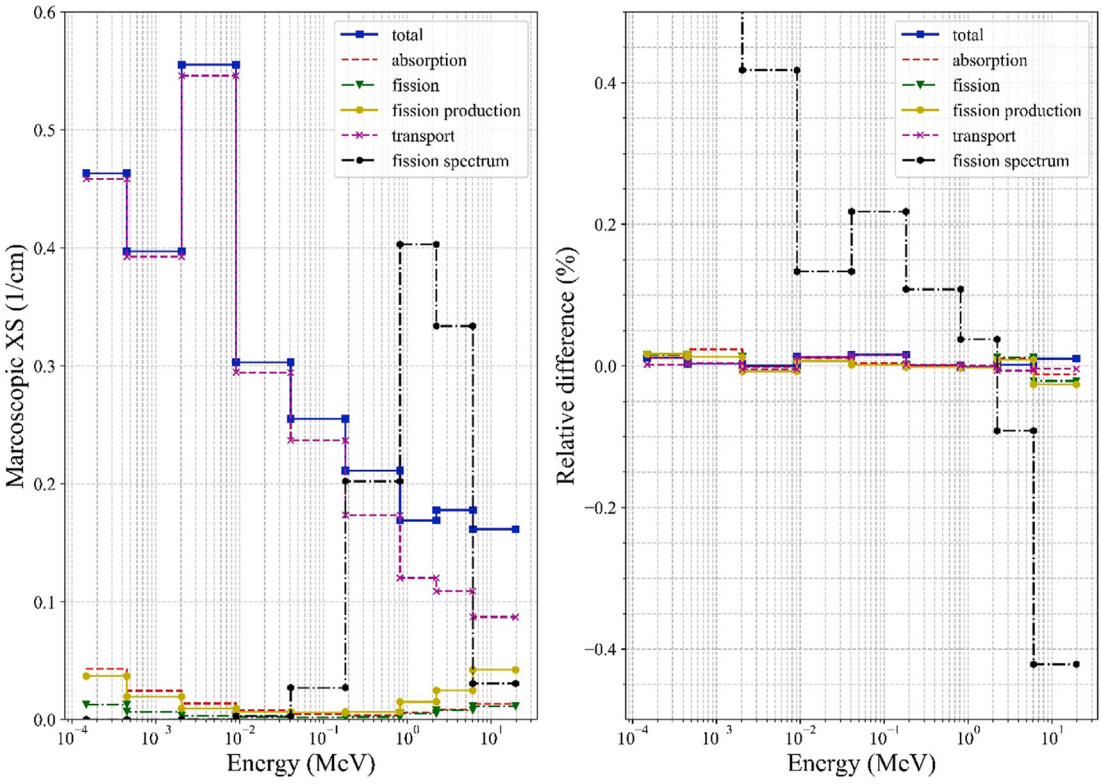

Fig. 6. Macroscopic XSs from MCS (left) and comparison with results of Serpent 2 (right).

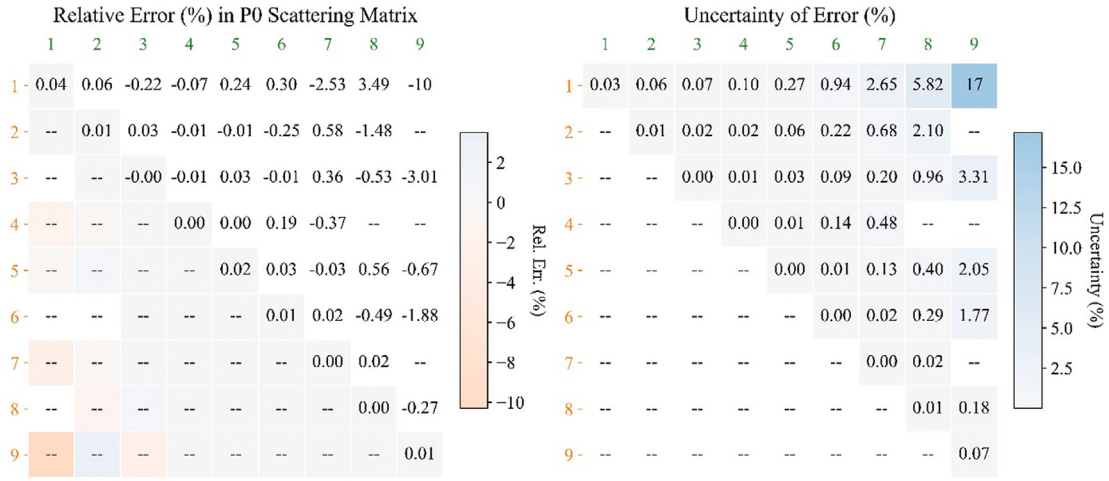

Fig. 7. Error in P0 scattering matrix (left) and uncertainties (right) for MCS and Serpent 2 results.

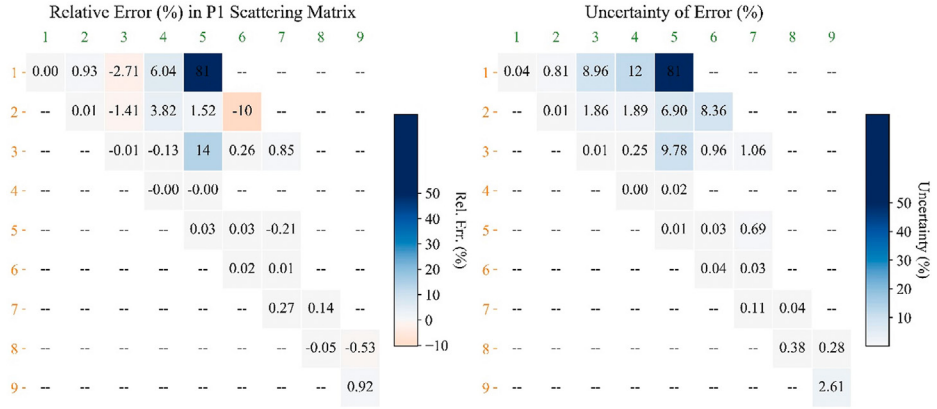

Fig. 8. Error in P1 scattering matrix (left) and uncertainties (right) for MCS and Serpent 2 results.

than 3D simulations as dealing with many types of SA. The two-step approach would allow users to generate a one-time assembly XS with the high-cost method (MC in this work), and then to run the many combinations of assemblies with the low-cost method (diffusion code, R2, in this case). This approach would be beneficial for core designs such as searching for optimized loading patterns rather than create the most accurate benchmark results. It is because of a large neutron mean-free path, the effect of the neighbor assemblies is more considerable than the light water reactors. To evaluate the accuracy of the fuel SA's XSs generated by the super cell model, the comparison of the flux spectrum of the fuel SA at several locations in the whole-core model with those in the super cell models is conducted and shown in Fig. 10. A rough consistency is observed in flux spectrum either in the super cell model or the whole-core model.

To better approximate that strong spectral shift effect at the fuel-reflector interface, a 2D radial reflector model (RRM) as shown in Fig. 11 is employed with the vacuum boundary at the right. This layout expects to give a better approximation of the flux spectrum that reflector SAs experienced in the core rather than the super cell model. It is then confirmed by the flux spectrum comparison, as the reflector SA is placed (i) in the super cell model, (ii) in the RRM, and (iii) in the whole-core model, which is illustrated in Fig. 12. Table 4 shows the comparison in k_{eff} as using reflector XS generated from those three models and Fig. 13 describes the corresponding error in radial power distribution with the MC whole-core model. It is seen that the use of the RRM for XS generation creates a better agreement in terms of reactivity and assembly power in the core periphery. As result, the reflector XS generated by the RRM is used for R2 3D core calculation.

The contribution of the axial leakage and the spectral shift is, however, expected to be negligible in terms of core reactivity. Further analysis on the axial spectral shift is conducted in the case of the MET-1000. Additional to the super cell model, the 3D fuel SA

Table 3
Twenty-four-group energy structure.

No.	Upper E (MeV)	Lower E (MeV)	No.	Upper E (MeV)	Lower E (MeV)
1	1.96403E+01	1.00000E+01	13	4.08677E−02	2.47875E−02
2	1.00000E+01	6.06531E+00	14	2.47875E−02	1.50344E−02
3	6.06531E+00	3.67879E+00	15	1.50344E−02	9.11882E−03
4	3.67879E+00	2.23130E+00	16	9.11882E−03	5.53084E−03
5	2.23130E+00	1.35335E+00	17	5.53084E−03	3.35463E−03
6	1.35335E+00	8.20850E−01	18	3.35463E−03	2.03468E−03
7	8.20850E−01	4.97871E−01	19	2.03468E−03	1.23410E−03
8	4.97871E−01	3.01974E−01	20	1.23410E−03	7.48518E−04
9	3.01974E−01	1.83156E−01	21	7.48518E−04	4.53999E−04
10	1.83156E−01	1.11090E−01	22	4.53999E−04	3.04325E−04
11	1.11090E−01	6.73795E−02	23	3.04325E−04	1.48625E−04
12	6.73795E−02	4.08677E−02	24	1.48625E−04	1.00001E−11

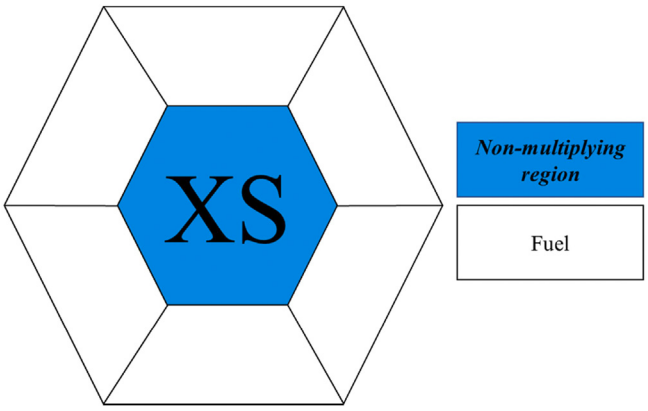

Fig. 9. 2D supercell model ("XS" indicates region where XSs are generated).

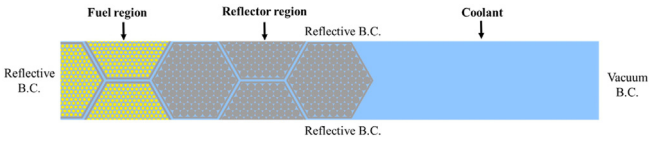

Fig. 11. Radial reflector model.

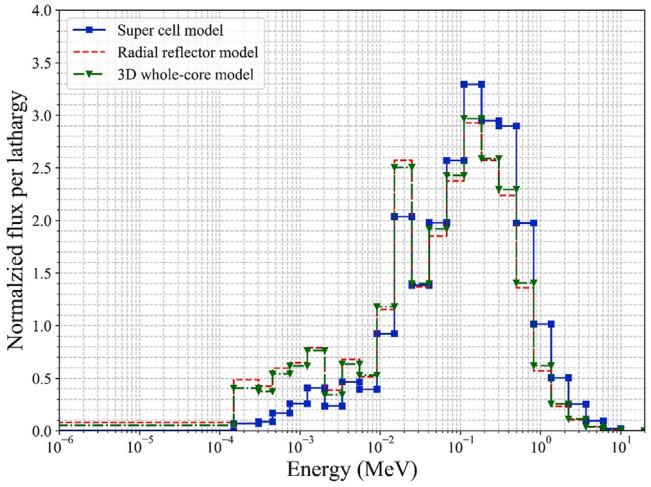

Fig. 12. Neutron flux spectrum at reflector SA for three different models.

model and the whole-core model are used to generate the XSs of the axial components of the reactor, such as bond sodium and lower reflector. The flux spectrum of the bond sodium and lower reflector for three different cases are compared and illustrated in Fig. 14. It is seen that the flux spectrum of those components in the 3D fuel SAs is consistent with those in the whole-core model. Even though those flux spectra in the whole-core model is quite different from those generated in the super cell models, the reactivity difference is negligible (less than 15 pcm) when comparing the k_{eff} obtained using the XS generated by super cell and the whole-core, as shown in Table 5. In fact, there is an error reduction in axial power distribution as shown in Fig. 15, especially at the bottom of the core where the spectral shift effect is considerable. It is also noted that the generation XS of the region that far from the active regions in the 3D whole-core model, such as the lower structure, is unreliable because of limited neutrons that are transported to such region resulting in unstable statistical uncertainties. It is likely an essential disadvantage as using 3D model for generating XS of non-multiplying regions. Overall, the 2D super cell model of the axial component seems to be adequate to predict the XSs. Further study should be conducted for searching for a more efficient model to generate the XSs for the axial component of the reactor.

Furthermore, the SPH method [5,6] is applied to correct the flux-volume-weighted XS of the strongly absorbing region and its surroundings, i.e., the control SA and its six-surrounding fuel SAs rather than all fuel SAs. The SPH factors are computed using MCS/R2 by a procedure indicated in Fig. 16. First, a supercell model of the control SA is employed to produce the heterogeneous transport solution of the fluxes and MG XSs of two regions, i.e., the control SA and its surroundings. Then, the equivalent R2 supercell model is

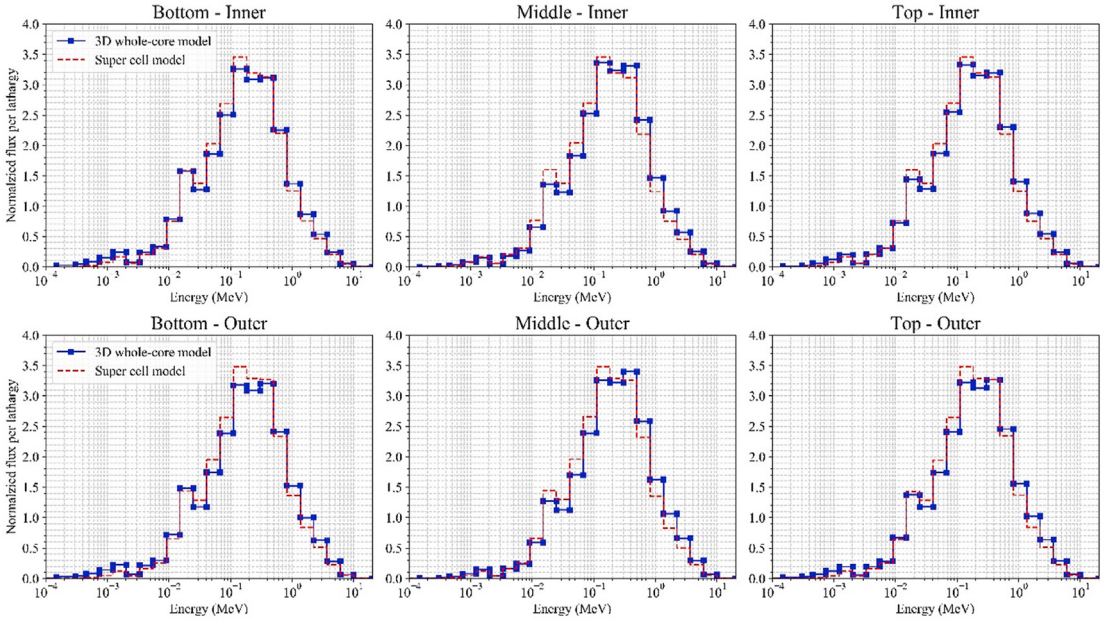

Fig. 10. Flux spectrum comparison of inner and outer fuel SA at several locations.

Table 4
k_{eff} comparison with reflector XS from three different model.

Case		k_{eff}	Diff. (pcm)
MCS whole core (±3σ)		1.02995 ± 0.00013	Reference
MCS/R2, reflector XS from:	(i) Super cell	1.03134	130
	(ii) Radial reflector	1.03039	41
	(iii)Whole-core	1.03046	48

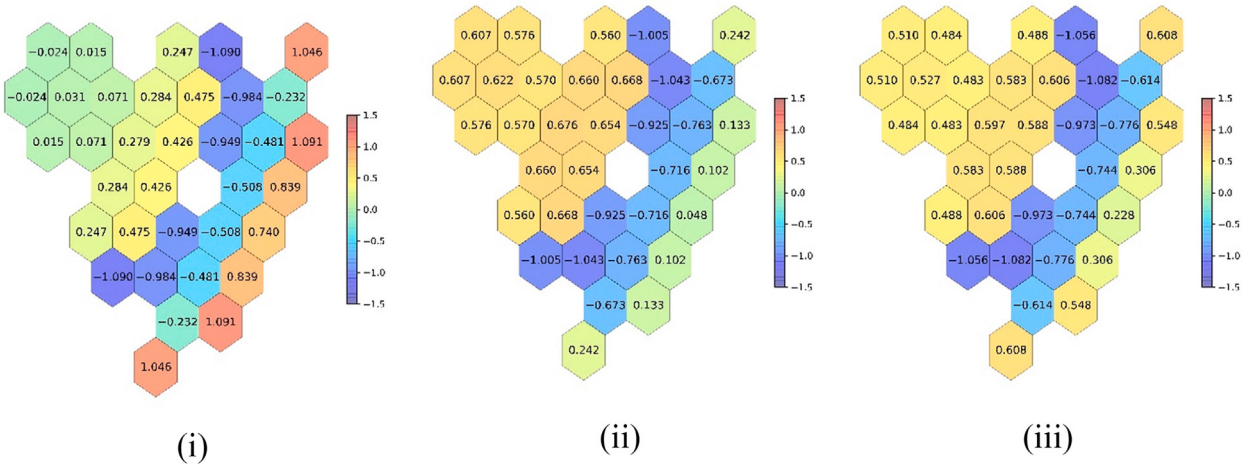

Fig. 13. Error in normalized radial power distribution with three different reflector XS from: (i) super cell model, (ii) radial reflector model and (iii) whole-core model.

generated (Fig. 17) to obtain the homogeneous region-wise diffusion fluxes. The SPH factors are then generated using an iterative method:

$$SPH_{r,g} = \frac{\overline{\phi}_{r,g}^{hete}}{\phi_{r,g}^{homo}} \times Norm_g, \text{ at } i^{th} \text{ iteration} \quad (7)$$

$$Norm_g = \frac{\sum_r V_r \phi_{r,g}^{homo}}{\sum_r V_r \overline{\phi}_{r,g}^{hete}} \quad (8)$$

where $\overline{\phi}_{r,g}^{hete}$ and $\phi_{r,g}^{homo}$ are the MCS average heterogeneous and R2 homogeneous flux in region r and group g, respectively, and $Norm_g$

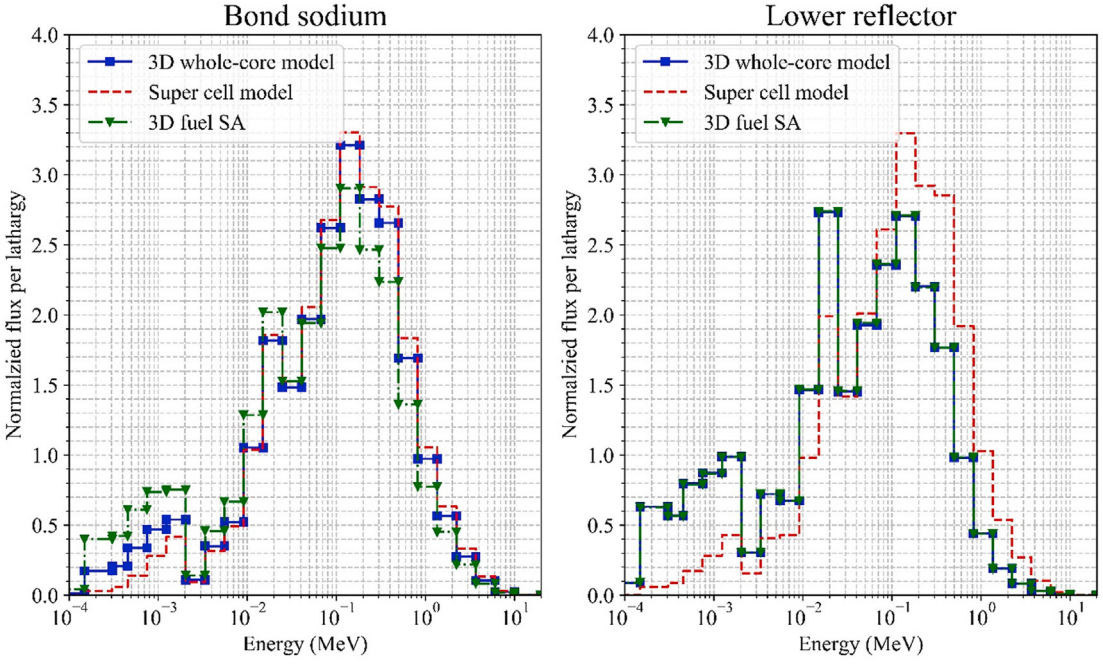

Fig. 14. Neutron flux spectrum at bond sodium and lower reflector in three different models.

Table 5
k_{eff} comparison with axial bond sodium and lower reflector XS from three different models.

Case		k_{eff}	Diff. (pcm)
MCS whole core (±3σ)		1.02995 ± 0.00013	Reference
MCS/R2, axial reflector XS from:	(i) Super cell	1.03039	41
	(ii) 3D fuel SA	1.03050	52
	(iii) Whole-core	1.03011	15

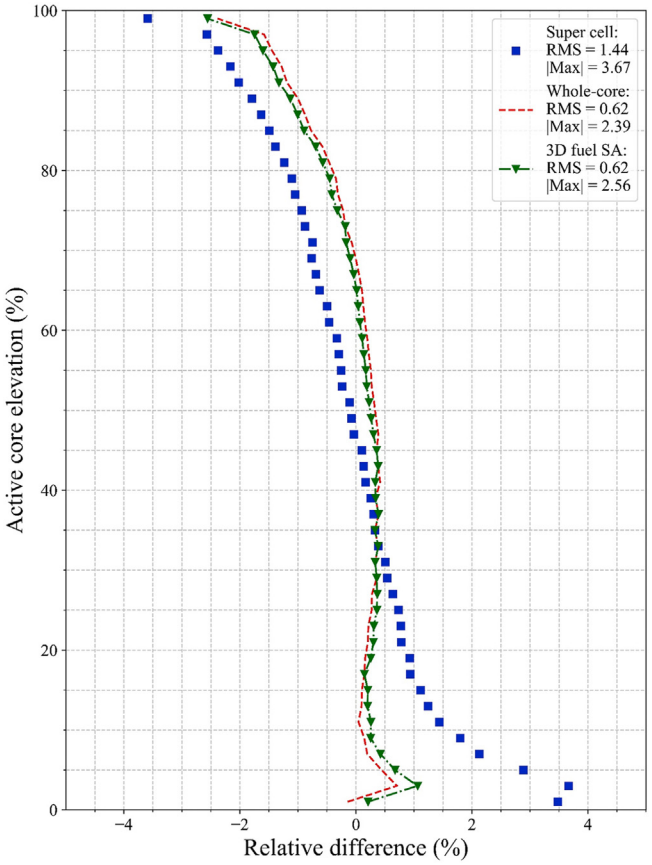

Fig. 15. Error in normalized power distribution as bond sodium and lower reflector XS generated from three different models.

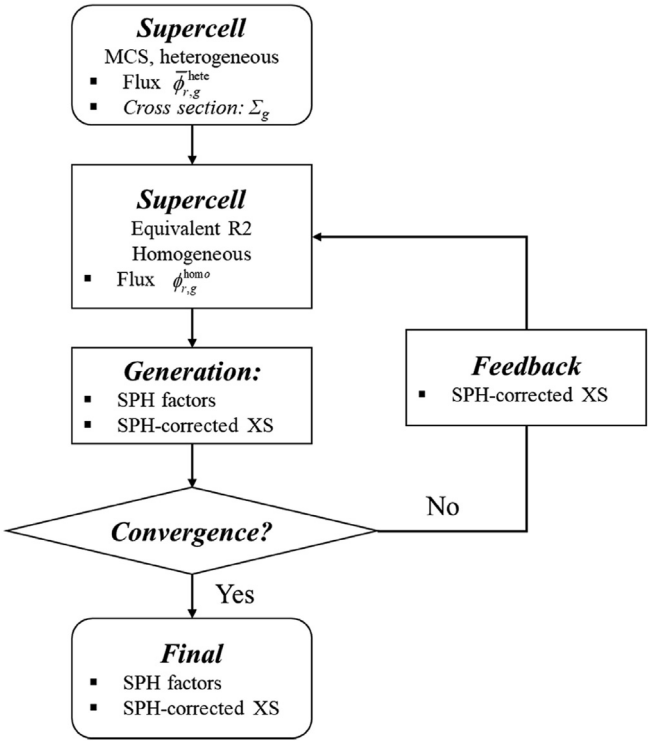

Fig. 16. Iteration scheme for SPH factor generation.

is a normalization factor, which is defined in Eq. (8). The modified XSs for each region and energy group are then produced using Eq. (9). Note that the fission spectrum remains unchanged during the iteration.

$$\Sigma^{mod}_{r,g} = SPH_{r,g} \times \Sigma_{r,g} \tag{9}$$

R2 repeats the simulation until the following conversion criterion is met:

$$\max \frac{\left|SPH^{i}_{r,g} - SPH^{i-1}_{r,g}\right|}{SPH^{i-1}_{r,g}} < 10^{-5} \tag{10}$$

For the normal non-multiplying regions, i.e., the gas plenum, axial reflector, and radial reflector, one supercell model is used to generate the XS. A supercell model based on the type of control SA and its location is created. The MET-1000 benchmark has only one type of control SA facing the inner and outer fuel SAs. Therefore, two supercell models are simulated. A total of 10 and 12 supercell models of the MET-1000 and MOX-3600 cores, respectively, are simulated. To run a single calculation of R2, 18 sets of macroscopic XS are required for a steady-state core model.

Fig. 18 shows the eigenvalue and SPH factor convergence behavior during the iteration for a MET-1000 control SA surrounded by six outer fuel SAs. The eigenvalue rapidly reaches the MCS reference solution after a few iterations and gradually becomes stable. The number of iterations required to make the SPH factor converge is case-dependent, and in the case of MET-1000 core, more than 20 iterations were required to satisfy the convergence criterion of less than 10^{-5}. Table 6 shows the SPH factors of the control SA and fuel SA for this example. After it is modified by the SPH factors, the control rod XS decreases by factors ranging from 0.58 to 0.90, whereas the fuel XS in the surrounding regions increases by factors of 1.01–1.03. For the two SFR core designs, the SPH factors converge to values ranging from 0.6 to 1.1 for all the energy groups.

In the whole-core problem, two approaches are used to apply the SPH factors. In one approach, the XS is modified only in the control SA regions, and in the other, the XS is modified in the control SA region and the surrounding fuel SAs. A detailed discussion is presented in the next section.

4.2. Numerical results

The 24-group macroscopic XS data are obtained by MCS and reconstructed into a database that is compatible with the nodal

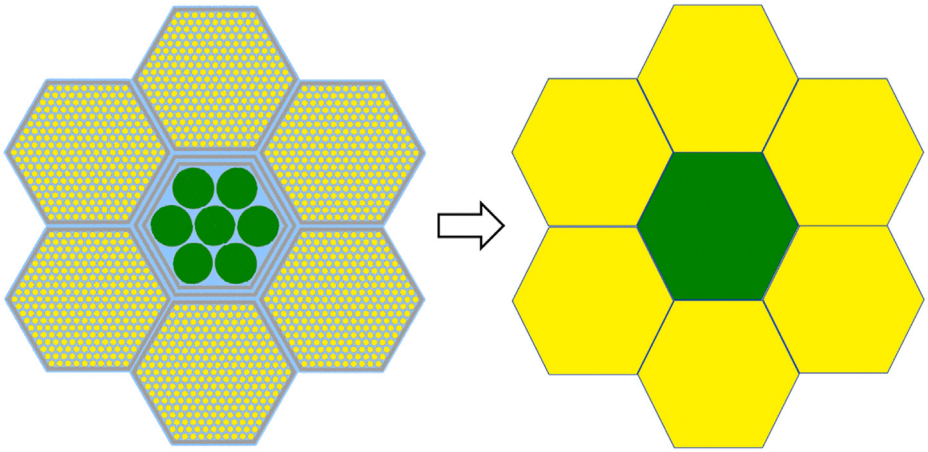

Fig. 17. Heterogeneous MCS (left) and equivalent homogeneous R2 (right) supercell models.

diffusion code R2 to simulate a whole-core problem and predict several parameters of interest, including the core multiplication factor (k_{eff}), fuel temperature coefficient (FTC), coolant temperature coefficient (CTC), total CRW, and power profiled with all rods out (ARO) and all rods in (ARI).

The FTC [19] is defined as the difference in reactivity per difference in fuel temperature, and it is calculated using Eq. (11) as follows:

$$FTC\ [\text{pcm/K}] = \frac{\Delta\rho}{\Delta T_f} = \frac{\rho_2 - \rho_1}{T_{f2} - T_{f1}} \tag{11}$$

where T_{f1} and T_{f2} are the nominal and perturbed fuel temperatures, respectively, and ρ_1 and ρ_2 are the corresponding reactivities. The CTC is defined as the change in reactivity due to change in the average coolant density [19]. The coolant density typically decreases with increasing coolant temperature. The CTC is calculated using Eq. (12) as follows:

$$CTC\ [\text{pcm/K}] = \frac{\partial\rho}{\partial\gamma}\frac{\partial\gamma}{\partial T} \approx \frac{\Delta\rho}{\Delta\gamma}\frac{\Delta\gamma}{\Delta T} = \frac{\Delta\rho}{\Delta T} \tag{12}$$

where $\Delta\gamma$ is the difference in the average coolant density for a difference ΔT in the average coolant temperature. The CRW is the total worth of all the control SAs and is calculated as the difference in reactivity between the ARO and ARI states [19]:

$$CRW\ [\text{pcm}] = \rho_{ARO} - \rho_{ARI} \tag{13}$$

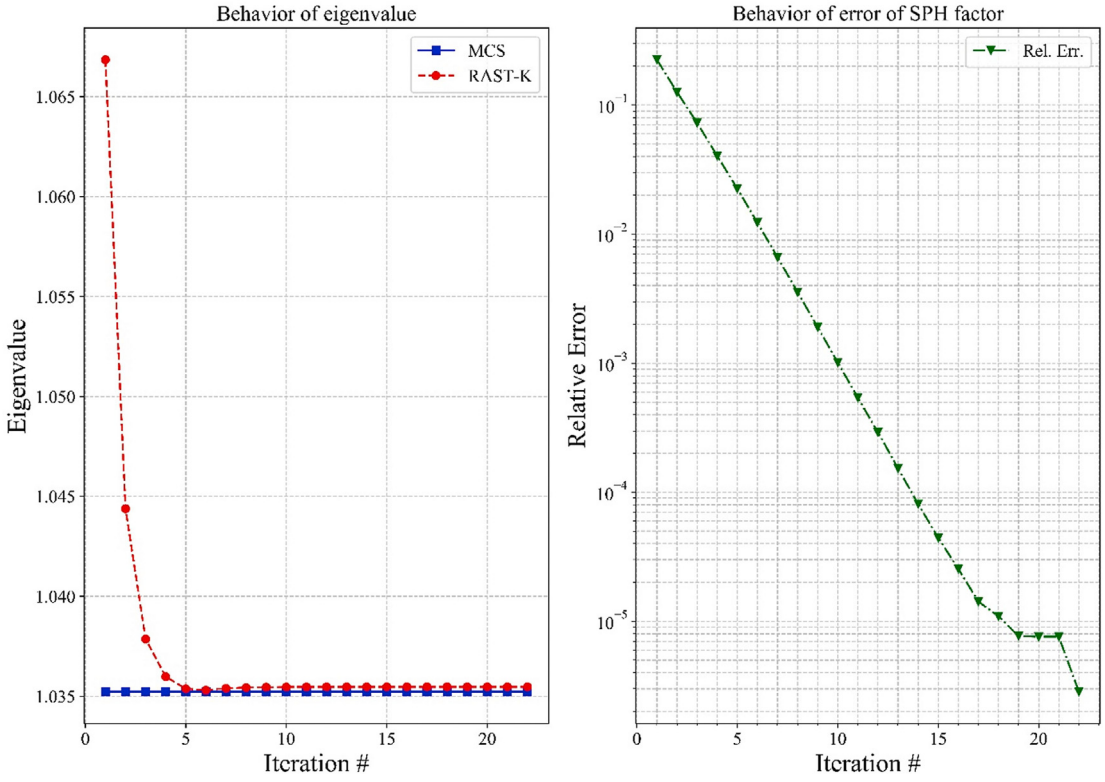

Fig. 18. Eigenvalue and SPH factor convergence during iteration.

Table 6
SPH factors of fuel and control SAs.

Group #	Fuel	Control	Group #	Fuel	Control
1	1.0307	0.7454	13	1.0117	0.8882
2	1.0286	0.7583	14	1.0149	0.8391
3	1.0253	0.7861	15	1.0177	0.8151
4	1.0214	0.8189	16	1.0189	0.7787
5	1.0185	0.8555	17	1.0197	0.7276
6	1.0171	0.8692	18	1.0204	0.7010
7	1.0167	0.8630	19	1.0239	0.6421
8	1.0159	0.8613	20	1.0267	0.6279
9	1.0143	0.8814	21	1.0295	0.6127
10	1.0130	0.8873	22	1.0303	0.6126
11	1.0124	0.8947	23	1.0364	0.5870
12	1.0126	0.8901	24	1.0286	0.6739

Table 7
MET-1000 core parameters calculated using MCS and MCS/R2.

Parameter	MCS ($\pm 3\sigma$)	MCS/R2	Diff. ($\pm 3\sigma$, %)
k_{eff}	1.02995 ± 0.00013	1.03039	0.042 ± 0.012
FTC (pcm/K)	−0.336 ± 0.041	−0.329	−2.2 ± 12.1
CTC (pcm/K)	0.540 ± 0.034	0.550	1.7 ± 6.3

Table 8
MOX-3600 core parameters calculated using MCS and MCS/R2.

Parameter	MCS ($\pm 3\sigma$)	MCS/R2	Diff. ($\pm 3\sigma$, %)
k_{eff}	1.01747 ± 0.00014	1.01856	0.107 ± 0.01
FTC (pcm/K)	−0.867 ± 0.039	−0.894	3.1 ± 4.5
CTC (pcm/K)	0.437 ± 0.038	0.418	−4.5 ± 8.6

The temperature-dependent XS is obtained using the interpolation module implemented in MCS. In addition, MCS employs probability table to consider the self-shielding effect in the unresolved energy range. The ENDF/B-VII.0 cross section library is used for all the simulations, where the temperatures of the fuel and the other materials are set to 900 and 600 K, respectively. The reference solutions are computed using MCS with the criticality set as follows: 5 inactive batches, 20 active batches, 200 cycles per batch, and 20,000 histories per cycle.

The k_{eff} values of MET-1000 and MOX-3600 obtained by 3D whole-core calculation using MCS/R2 and MCS at the beginning of the cycle with ARO are summarized in Tables 7 and 8, respectively. Figs. 19 and 20 show the radial assembly-wise power and axial power distributions of MET-1000 and MOX-3600 with ARO calculated by MCS/R2 and MCS. The standard deviations (SDs) of the radial power and axial power obtained by MCS are summarized in Table 9. The results for both benchmark cores are clearly in excellent agreement; the difference in k_{eff} is less than 110 pcm, the root-mean-square (RMS) error of the radial power is less than 0.7%, and that of the axial power is less than 1.5%. It is seen that the peak in axial power errors appears at the top and bottom of the core. This is because of the use of 2D reflective-boundary model for the axial component of fuel SAs that results in the underestimate of neutron leakage and spectral shifting effect. However, negligible errors are introduced to the whole-core simulation results. Additional analysis on the reactivity feedback coefficients predicted by MCS/R2 (the FTC and CTC) shows a good agreement with those predicted by MCS, as the differences are within three SDs.

Table 10 summarizes the CRWs calculated by MCS and MCS/R2. When no correction is applied, R2 clearly overestimates the effect of the control SAs with ARI, by approximately 15% for MET-1000 and 5% for MOX-3600. Better solutions are obtained when the SPH factor is applied only in the control rod region, but the difference in the CRW remains large, approximately 5.6% for MET-1000 and 1.7% for MOX-3600. When the SPH-corrected XSs are used for both the control SA and its surrounding SAs, the R2 solutions apparently converge to the MCS rod worth, as the error decreases to less than 0.6% for both cores. The error originates mainly from the control rod XS, and further improvement is obtained when the correction is introduced to its surrounding regions. This analysis suggests that the SPH factor should be applied to both the control SAs and their surrounding fuel SAs. When the SPH factor is applied, not only the CRW but also the radial power distribution is predicted more accurately. Figs. 21 and 22 present the radial power distributions of the MET-1000 and MOX-3600 cores without and with the SPH factors. An overall decrease in the RMS and maximum power error is clearly observed. SPH correction is thus essential for highly accurate analyses of fast reactors.

To evaluate the transport effect and to determine whether the error cancellation occurs, an additional analysis is performed by the MCS MG transport solver using the same XS set in the diffusion solver R2. Table 11 summarizes the core k_{eff} obtained by MG diffusion solver and MG transport solver compared to MCS 3D whole-core results. It is noted that only P0 transport-corrected scattering matrix is used in MCS MG transport calculation, which is the same approach in the diffusion solver. In comparison to the MG transport calculation, the diffusion calculation underestimates the k_{eff} by more than 300 pcm for large-size MOX-3600 core, and the difference in k_{eff} becomes more significant (more than 1000 pcm) for small-size MET-1000 core. Indeed, there is an interesting error cancellation as using the diffusion calculation, owning to the fact that the error from the XS might be compensated by the underestimation of core reactivity. The source of error in XS may come from the transport XS as the out-flow transport correction was used, which requires the P1 scattering matrix. The P1 scattering matrix in this study is weighted only by the scalar flux rather than the angular flux, which can create errors in the transport XS (converted to diffusion coefficient in R2). Further comparison in the radial power distribution is illustrated in Fig. 23 and indicates that there is a tilt in the relative differences between the two solvers. The diffusion solver seems to overestimate the power in the core center while underestimating the power in the core periphery compared to the transport solver. There are insignificant errors in axial power profiles so that it is not included in this discussion. Overall, the occurrence of such an error cancellation might be in the favorable tendency when using the XS generated by the MC method. However, a more rigorous study should be conducted to evaluate how the error cancellation happens in diffusion solver and to ensure the reliability and stability of the MC-diffusion code sequence against various fast reactor designs.

5. Conclusions

The feasibility of using the MCS MC code to generate macroscopic MG XSs for fast 3D spectral simulations using R2 simulators is investigated. A few-group XS tallied by MCS shows excellent agreement with Serpent 2 solutions. To quantify the XS generation feature in MCS in a whole-core study, steady-state analyses by R2 using 24-group XS data are conducted to predict the core k_{eff}, power profiles, and reactivity coefficients. A code-to-code comparison shows excellent agreement between the results of MCS/R2 and MCS; the k_{eff} bias is less than 110 pcm, and the RMS differences in the radial and axial power are less than 0.7% and 1.5%, respectively. Moreover, the reactivity feedback coefficient (the FTC and CTC) calculated by MCS/R2 are in good agreement with those calculated by MCS, as the errors are within three SDs. The SPH method is studied further by calculating the CRW. Applying the SPH factors improves the accuracy of the CRW (less than 0.7%) and reduces the

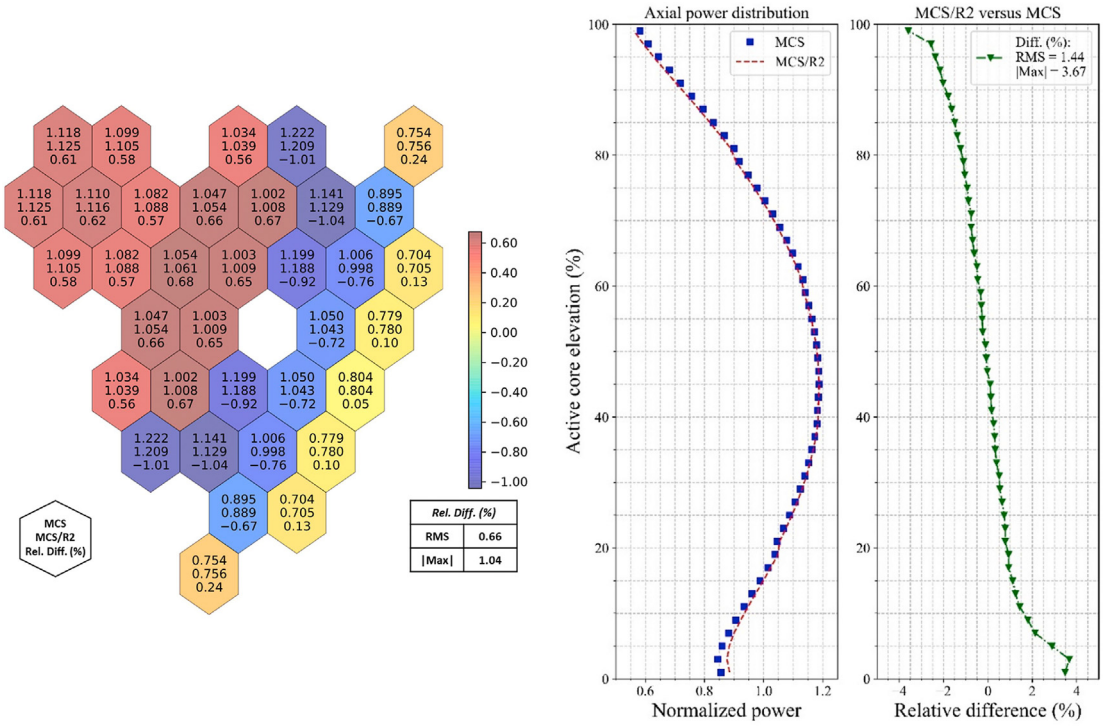

Fig. 19. Radial power distribution (for one-sixth core symmetry, left) and axial power distribution (right) of MET-1000 calculated by MCS/R2 and MCS.

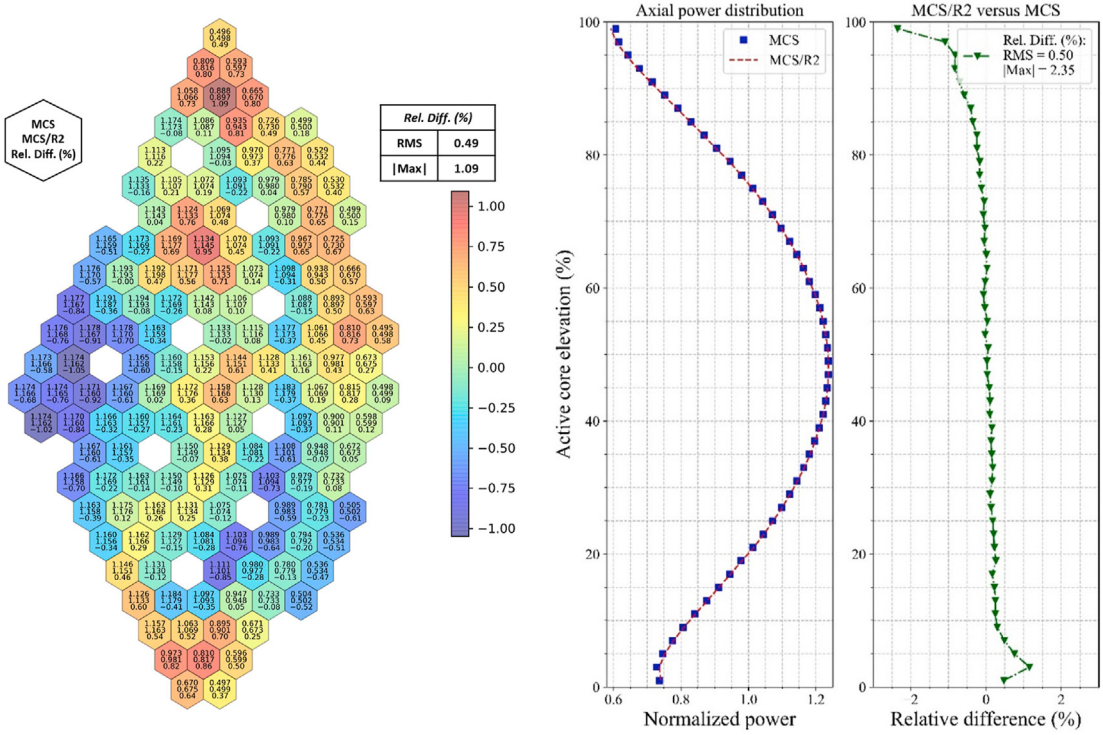

Fig. 20. Radial power distribution (for one-third-core symmetry, left) and axial power distribution (right) of MOX-3600 calculated by MCS/R2 and MCS.

RMS error of the radial power. In conclusion, the results of this study prove that the MCS could be a promising tool for MG XS generation for fast reactor analysis. This success was built owing to the nature of the MC method in the capability of generating XSs for the arbitrary geometry and material composition in the arbitrary few-group energy structure. Those few-group XSs were directly collapsed from the continuous energy without introducing any significant mathematical approximations, especially in self-shielding and resonance treatment, compared to the deterministic approach. Because of a large neutron mean free path in fast reactors, the effect of neighbor assemblies on the target flux spectrum is considerable. Therefore, the considerable radial

Table 9
Relative SD in power profiles tallied by MCS.

Power SD (%)	MET-1000		MOX-3600	
	Radial	Axial	Radial	Axial
Max.	0.22	0.04	1.27	0.07
Avg.	0.15	0.03	0.84	0.04

leakage and spectral shift in fast spectrum reactors are addressed by replacing the super cell model with the RRM. Another significant contribution to the great fast reactor analysis is applying the SPH method to corrects XSs in the strong absorber region and its surroundings, resulting in the great prediction of the CRW. Apparently, a favorable occurrence of the error cancellation shows that the

Table 10
CRWs obtained using MCS/R2 and MCS.

Case	MCS (±3σ pcm)	Without SPH		With SPH (only control rod)		With SPH (control rod + fuel)	
		MCS/R2 (pcm)	Diff. (pcm/%)	MCS/R2 (pcm)	Diff. (pcm/%)	MCS/R2 (pcm)	Diff. (pcm/%)
MET-1000	18,270 ± 20	20,951	**2681/14.7**	19,287	**1017/5.6**	18,180	***−90/−0.5***
MOX-3600	5954 ± 16	6241	**286/4.8**	6054	**99/1.7**	5989	***35/0.6***

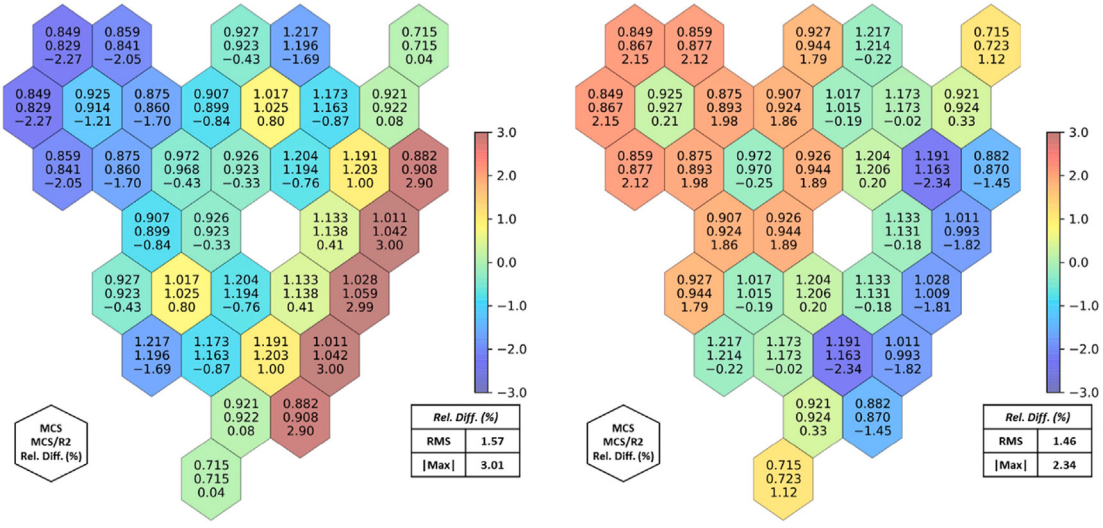

Fig. 21. Radial power distribution (for one-sixth core symmetry) of MET-1000 without SPH factors (left) and with SPH factors (right) calculated by MCS/R2 and MCS.

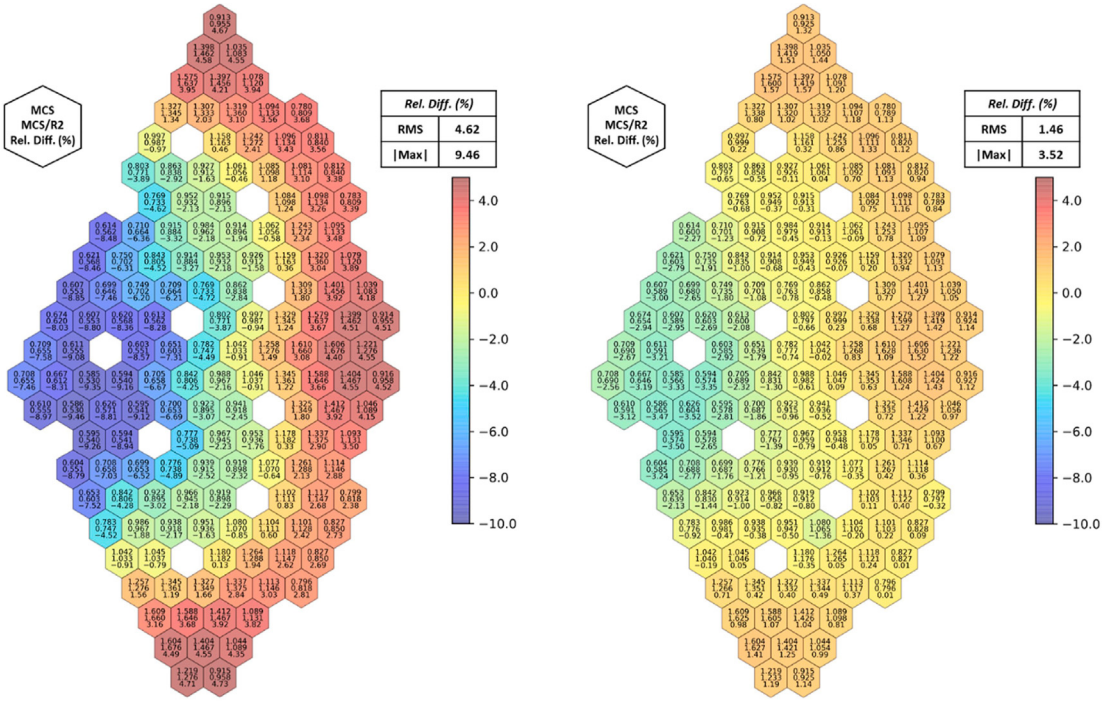

Fig. 22. Radial power distribution (for one-third core symmetry) of MOX-3600 without SPH factors (left) and with SPH Factors (right) calculated by MCS/R2 and MCS.

Table 11
Comparison of diffusion and transport calculations.

Case	MCS (Ref., ±5 pcm)	MCS/R2 (MG Diffusion)		MCS/MCS (MG transport)	
		k_{eff}	Diff. (±5 pcm)	k_{eff} (±8 pcm)	Diff. (±9 pcm)
MET−1000	1.02995	1.03039	41	1.04159	1085
MOX−3600	1.01747	1.01856	105	1.02209	444

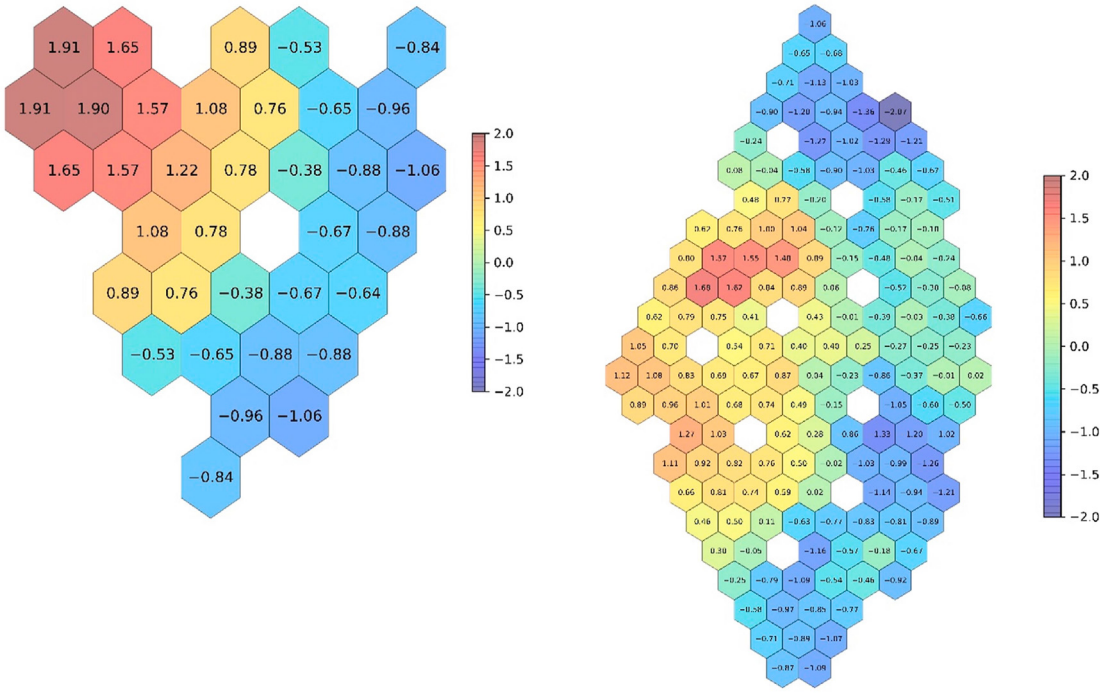

Fig. 23. Radial power distribution comparison between transport solver and diffusion solver: MET-1000 (for one-sixth core symmetry, left) and MOX-3600 (for one-third core symmetry, right).

diffusion solver underestimates the core reactivity that might be compensated by the XS error. Various points essential to the feasibility of this approach, however, are left as future work and require rigorous studies. Further study in the transport effect and the error cancellation sources should be properly conducted to ensure the reliability and stability of the suggested code sequence, MCS/R2, against diverse fast reactor designs. The high-order scattering matrices in this study are weighted only by the scalar flux rather than the angular flux. The functional expansion tally of the angular flux and high-order scattering matrices should be addressed in a later study. The benchmark cores do not contain any blanket/breeding material, and no moderating material is present in the reflector region. The effects of these materials on the use of the homogenized XS over a large volume should be studied using another core design. Complex T/H and transient phenomena may significantly affect fast reactor operation. Therefore, the application of MCS, coupled with T/H feedback, to generate the temperature-dependent and coolant-density-dependent microscopic XSs for burnup calculations in fast reactor analysis is left as future work.

Declaration of competing interest

The authors declare that they have no known competing financial interests or personal relationships that could have appeared to influence the work reported in this paper.

Acknowledgments

This work was supported by the National Research Foundation of Korea (NRF) grant funded by the Korea government (MSIT). (No.NRF-2017M2A8A2018595).

References

[1] J.E. Kelly, Generation IV International Forum: a decade of progress through international cooperation, Prog. Nucl. Energy 77 (2014) 240–246.
[2] E. Nikitin, E. Fridman, K. Mikityuk, Solution of the OECD/NEA neutronic SFR benchmark with Serpent-DYN3D and Serpent-PARCS code systems, Ann. Nucl. Energy 75 (2015) 492–497.
[3] E. Nikitin, E. Fridman, Extension of the reactor dynamics code DYN3D to SFR applications—Part II: validation against the Phenix EOL control rod withdrawal tests, Ann. Nucl. Energy 119 (2018) 411–418.
[4] W. Heo, W. Kim, Y. Kim, S. Yun, Feasibility of a Monte Carlo-deterministic hybrid method for fast reactor analysis, in: Proceedings of the 2013 International Conference on Mathematics and Computational Methods Applied to Nuclear Science and Engineering - M&C 2013, Idaho, USA, May 5–9, 2013.
[5] E. Nikitin, E. Fridman, K. Mikityuk, On the use of the SPH method in nodal diffusion analyses of SFR cores, Ann. Nucl. Energy 85 (2015) 544–551.
[6] R.S. Sen, A.J. Hummel, H. Hiruta, *SuPer-Homogenization (SPH) Corrected Cross Section Generation For High Temperature Reactor* (No. INL/EXT-17-41516), Idaho National Laboratory, Idaho Falls, ID (United States), 2017.
[7] H. Lee, W. Kim, P. Zhang, M. Lemaire, A. Khassenov, J. Yu, Y. Jo, J. Park, D. Lee, MCS—A Monte Carlo particle transport code for large-scale power reactor analysis, Ann. Nucl. Energy 139 (2020), 107276.
[8] T.D.C. Nguyen, H. Lee, S. Choi, D. Lee, Validation of UNIST Monte Carlo code MCS using VERA progression problems, Nucl. Eng. Technol. 52 (5) (2020) 878–888.

[9] J. Jang, W. Kim, S. Jeong, E. Jeong, J. Park, M. Lemaire, H. Lee, Y. Jo, P. Zhang, D. Lee, Validation of UNIST Monte Carlo code MCS for criticality safety analysis of PWR spent fuel pool and storage cask, Ann. Nucl. Energy 114 (2018) 495–509.
[10] T.M.N. Nguyen, Y. Jo, H. Lee, A. Cherezov, D. Lee, Whole-core Monte Carlo analysis of MOX-3600 core in NEA-SFR benchmark using MCS code, in: Proceedings of the Korean Nuclear Society Autumn Meeting, Yeosu, Korean, October 25–26, 2018.
[11] T.D.C. Nguyen, H. Lee, S. Choi, D. Lee, MCS/TH1D analysis of VERA whole-core multi-cycle depletion problems, Ann. Nucl. Energy 139 (2020), 107271.
[12] V. Dos, H. Lee, J. Choe, M. Lemaire, H.C. Shin, H.S. Lee, D. Lee, Verification & validation of MCS multi-physics analysis capability for OPR-1000 multi-cycle operation, in: Proceedings of the 2019 International Conference on Mathematics and Computational Methods Applied to Nuclear Science and Engineering - M&C 2019, Oregon, USA, August 25–29, 2019.
[13] T.D.C. Nguyen, H. Lee, J. Choe, M. Lemaire, D. Lee, APR-1400 whole-core depletion analysis with MCS, in: Proceedings of the 2019 International Conference on Mathematics and Computational Methods Applied to Nuclear Science and Engineering - M&C 2019, Oregon, USA, August 25–29, 2019.
[14] J. Choe, S. Choi, P. Zhang, J. Park, W. Kim, H.C. Shin, H.S. Lee, J.-E. Jung, D. Lee, Verification and validation of STREAM/RAST-K for PWR analysis, Nucl. Eng. Technol. 51 (2) (2019) 356–368.
[15] T.Q. Tran, A. Cherezov, X. Du, J. Park, D. Lee, Development of hexagonal-Z geometry capability in RAST-K for fast reactor analysis, in: 19th International Conference on Emerging Nuclear Energy Systems (ICENES 2019), Bali, Indonesia, October 6–9, 2019.
[16] J. Leppänen, M. Pusa, E. Fridman, Overview of methodology for spatial homogenization in the Serpent 2 Monte Carlo code, Ann. Nucl. Energy 96 (2016) 126–136.
[17] N.E. Stauff, T.K. Kim, T.A. Taiwo, et al., *Benchmark For Neutronic Analysis of Sodium-Cooled Fast Reactor Cores With Various Fuel Types and Core Sizes* (No. NEA-NSC-R–2015-9), Organization for Economic Co-Operation and Development, 2016.
[18] W.R.D. Boyd III, Reactor agnostic Multi-Group Cross Section Generation for Fine-Mesh Deterministic Neutron Transport Simulations, doctoral dissertation, Massachusetts Institute of Technology, 2017.
[19] L. Ghasabyan, Use of Serpent Monte-Carlo Code for Development of 3D Full-Core Models of Gen-IV Fast-Spectrum Reactors and Preparation of Group Constants for Transient Analyses with PARCS/TRACE Coupled System, master of science thesis, Royal Institute of Technology, KTH, 2013.